The Influence of Shape on the Stresses in Model Abdominal Aortic Aneurysms

D. F. Elger

D. M. Blackketter

R. S. Budwig

Mechanical Engineering Dept.,
University of Idaho,
Moscow, Idaho 83844-0902

K. H. Johansen
Univ. of Washington,
School of Medicine,
Seattle, WA 98195

Presence of a small abdominal aortic aneurysm (AAA) often presents a difficult clinical dilemma--a reparative operation with its inherent risks versus monitoring the growth of the aneurysm, with the accompanying risk of rupture. The risk of rupture is conventionally believed to be a function of the AAA bulge diameter. In this work, we hypothesized that the risk of rupture depends on AAA shape. Because rupture is inevitably linked to stress, membrane theory was used to predict the stresses in the walls of an idealized AAA, using a model which was axisymmetric and fusiform, with the ends merged into straight open-ended tubes. When the stresses for many different shapes of model AAAs were examined, a number of conclusions became evident: (i) maximum hoop stress typically exceeded maximum meridional stress by a factor of 2 to 3 (ii) the shape of an AAA had a small effect on the meridional stresses and a rather dramatic effect on the hoop stresses, (iii) maximum stress typically occurred near the inflection point of a curve drawn coincident with the AAA wall, and (iv) the maximum stress was a function--not of the bulge diameter--but of the curvatures (i.e. shape) of the AAA wall. This last result suggested that rupture probability should be based on wall curvatures, not on AAA bulge diameter. Because curvatures are not much harder to measure than bulge diameter, this concept may be useful in a clinical setting in order to improve prediction of the likelihood of AAA rupture.

Dilatation of the human abdominal aorta, called an abdominal aortic aneurysm or AAA (see Fig. 1(*a*)), is a common clinical problem, occurring in about 2 percent of the population, generally in older males. Other risk factors include hypertension, large body size and a positive family history. AAA natural history has been reviewed by Johansen (1982) and by Dobrin (1989). The major health threat of an AAA is rupture. When an AAA ruptures, 50 percent of patients die before reaching the operating room, and 54 percent of those who reach the operating room alive will die within 30 days (Katz, et al., 1992). Thus, AAA rupture is the 15th leading cause of death in the United States (U.S. Government Printing Office, 1991).

Physicians diagnose AAAs by physical exam, CT scan, or ultrasound, with the later method being the most common. Once an AAA has been detected, it may be replaced by insertion of an in-line prosthetic graft (aneurysmorrhaphy). This elective surgery has a mortality rate of about 4 to 5 percent (Katz, et al., 1992). Alternatively, when the risk of rupture is believed to be low, a physician may "watchfully wait." Watchful waiting involves regular ultrasound examination of the AAA bulge diameter (D_b on Fig. 1(*b*)), with operation proposed if D_b exceeds about 5 cm.

It is widely presumed that the risk of AAA rupture correlates with D_b, based on the law of Laplace (Johansen, 1982; Dobrin, 1989)[1]:

$$\sigma = \frac{pD_b}{4t}, \qquad (1)$$

where σ is the stress in the vascular wall, p is pressure and t is wall thickness. Eq. (1), which is valid for a thin-walled spherical pressure vessel, shows that maximum stress in a sphere correlates directly with the sphere diameter.

Insights about AAAs have been established by a succession of clinical studies. Prior to the advent of surgical resection, Estes (1950) used data from 102 patients with artheriosclerotic AAAs to describe the natural history and to assess survival rates as compared to the normal population. Surgical resection was established by Dubost et al. (1952), and since this time the relevant issue has been the timing of surgical intervention.

Bernstein et al. (1976), in a six year study, tracked poor-surgical-risk patients who had small asymptomatic AAAs. They reported three indications for surgery: enlargement to 6 cm. in any transverse diameter, the development of symptoms, or evidence of a leak or rupture. Cronenwett, et al. (1985) studied rupture by using statistical methods to analyze thirty potential risk factors. Based on a sample size of sixty-seven patients, they reported that rupture was predicted by only three of the factors analyzed: initial aneurysm anteroposterior diameter, diastolic blood pressure, and the degree of obstructive pulmonary disease. Several studies have related structural features to AAA growth and rupture. Hunter et al. (1989) and Faggioli et al. (1994) suggested that blebs (localized blisters on an AAA) may be a potential site for rupture. However, Faggioli et al. note that blebs only occur on small aneurysms in about 10 percent of cases. Veldenz et al. (1994), using CT data from nineteen AAA patients, showed that rapid expansion in aneurysm size correlates with wall curvatures.

Hollier et al. (1992) review the contemporary clinical treatment of AAAs. While many clinical studies have been performed, the optimal management of small AAAs ($D_b < 5$ cm) is still controversial and hence, is an area of active conjecture (Michaels, 1992; Katz et al., 1992; Brown, et al., 1992). The present need continues to be the timing of surgical intervention in order to minimize the risk, from both surgery and rupture, to a patient. While prior studies have applied statistical methods to retrospective and prospective clinical observations, we ap-

Contributed by the Bioengineering Division for publication in the Journal of Biomechanical Engineering. Manuscript received by the Bioengineering Division January 22, 1995; revised manuscript received July 11, 1995. Associate Technical Editor: F. C. P. Yin.

[1] Following the Johansen and Dobrin papers, the law of Laplace will refer to Eq. (1). Historically, the law of Laplace related pressure, stress and surface tension at the free surface of a liquid; e.g., see Fung (1993).

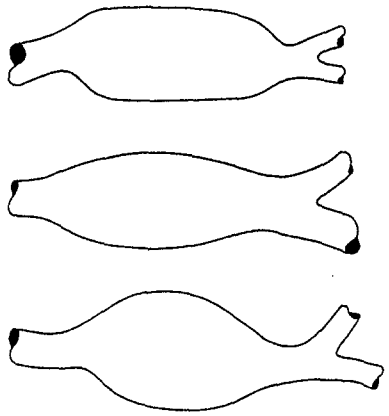

Fig. 1(*a*) Typical shapes of AAAs

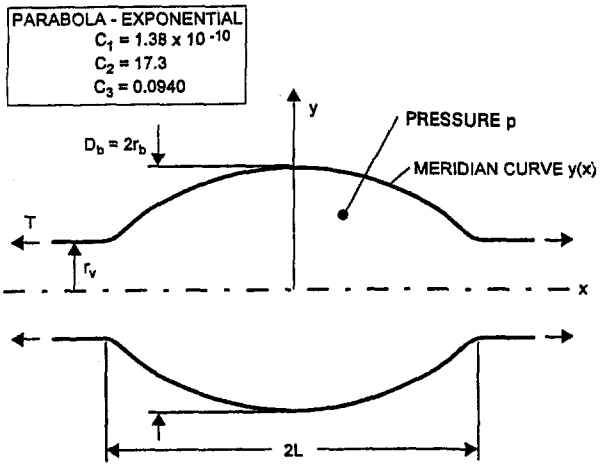

Fig. 1(*b*) an example of a model AAA

Fig. 1

proached the problem by studying AAA mechanics. In particular, we hypothesized that the risk of AAA rupture was related to the shape of the aneurysm.

The concept that AAA shape could influence growth and rupture has been proposed by Gaylis (1983) and by Stringfellow et al. (1987). To study this problem, Stringfellow et al. used the finite-element method (FEM) to predict the stresses in several AAAs, modeling the AAA as a thin-walled, axisymmetric, spherical or cylindrical pressure vessel with end tubes attached. They clearly showed that the AAA shape influences the stress distribution and that the law of Laplace is inaccurate. However, Stringfellow et al.'s analyses had a major problem: their models had constant wall curvatures and sharp corners where the bulge joined the nondilated aorta, causing misleading stress distributions.

To improve on Stringfellow et al's (1987) model, Mower et al. (1993) used a smooth shape and then calculated stresses using the FEM. Their model was axisymmetric and fusiform with thick-walls. They also concluded that the law of Laplace is inaccurate, and they reached several conclusions about the nature of the stress distribution: wall stresses are greatest on the inner surface and have a nonlinear variation through the wall thickness, and hoop stresses tend to be significantly greater than meridional stresses. The major limitation of Mower et al.'s work is that they varied both bulge diameter and wall curvatures simultaneously and thus did not determine how stress was related to AAA shape.

In summary, the previous studies have provided valuable information. However, only a limited number of AAA shapes were analyzed, and a number of the subsequent conclusions are either misleading or incorrect. In addition, these studies have not provided insight into why stress is influenced by AAA shape. This paper addresses these issues by using an analytical model to clarify how AAA shape affects the stress distributions.

Methods

AAA Models. AAAs display a variety of shapes, some of which are shown in Fig. 1(*a*). Our models idealize AAA shape as shown in Fig. 1(*b*). The AAA walls are assumed to have a uniform thickness, and to carry stresses by membrane action. Loads acting on the AAA wall are due to pressure exerted by the blood and tethering to surrounding tissues. To represent blood pressure, a steady uniform pressure p acts on the AAA walls. To represent perivascular tethering, an axial load T acts longitudinally on the model.

The model AAAs were selected based on two criteria: shapes used to illuminate the nature of the stress field, and shapes intended to be realistic. This latter objective was met by selecting model AAAs with wall curvatures similar to curvatures of real AAAs. Each model AAA required specification of a meridional curve, the details of which are presented in Appendix A. To identify each model, the name of the meridional curve is given (e.g., "Parabola-Exponential" on Fig. 1(*b*)), along with values of adjustable parameters (C_1, C_2 and C_3) used in the mathematical representation.

To select the dimensions of the AAA models, several factors were considered. Most models were selected with a bulge radius of $r_b = 2.5$ cm, and a tube radius of $r_v = 1$ cm. The bulge radius of 2.5 cm is the critical diameter for the surgery versus watchful-wait decision. The tube radius of 1 cm is an approximation based on data by Langewouters et al. (1984). They measured 20 abdominal aortas in vitro and reported an average inner radius of 0.85 cm with a standard deviation of 0.1 cm. To select the aspect ratio $L/r_v \approx 4$, we examined a casting shown in Drexler and Hoffman (1985), and radiograms shown in Kerstein et al. (1983) and Horwitz et al. (1985).

Stress Analysis. Stress analysis follows the standard methods used for axisymmetric thin shells (e.g., Hass, 1962; Ugural, 1981; or Flügge, 1973), using the geometry shown in Fig. 2. The unit-meridional-force N_ϕ acts in a direction parallel to the meridian curve and has units of force per length, with stress equaling N_ϕ/t, where t is wall thickness. To simplify nomenclature, we label N_ϕ the "meridional stress." Similarly, N_θ has units of force per length and acts in a direction tangent to a parallel of latitude; we call N_θ the "hoop stress."

The principal radii of curvature r_1 and r_2 characterize the shape of the AAA wall. Radius r_1 is perpendicular to the stress element, and its length equals the radius of curvature of $y(x)$:

$$r_1 = \frac{[1 + (dy/dx)^2]^{3/2}}{-(d^2y/dx^2)}. \tag{2}$$

Here, r_1 is positive when $y(x)$ has downward curvature. Radius r_2 is perpendicular to the stress element and extends to the axis of symmetry (x-axis). This radius can be visualized as providing the curvature for the axisymmetric shape. From Fig. 2(*c*),

$$r_2 = \sqrt{h^2 + y^2}, \quad \text{and} \tag{3}$$

$$\tan(\phi) = y/h = -1/(dy/dx). \tag{4}$$

Combining Eqs. (3) and (4) gives

$$r_2 = y(1 + (dy/dx)^2)^{1/2}. \tag{5}$$

Stress equations were found using static equilibrium. Summing forces normal to the stress element shown in Fig. 2(*d*) gave

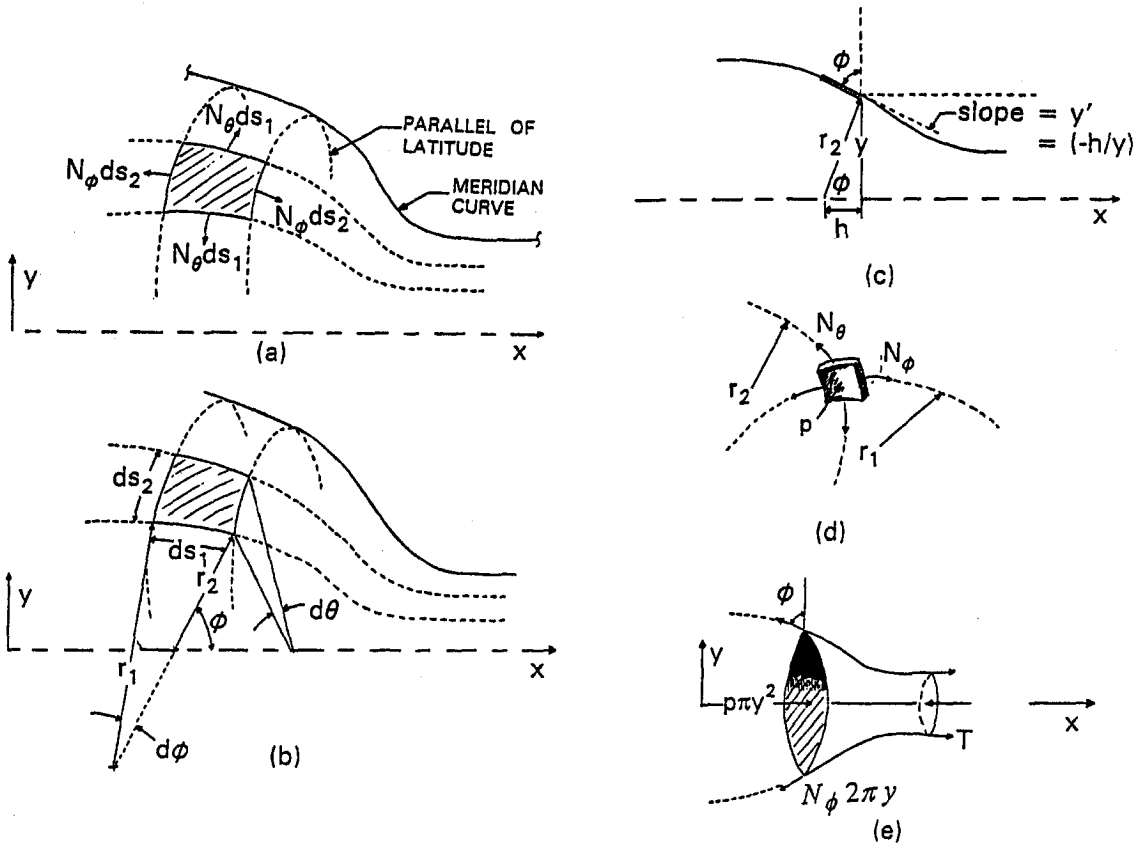

Fig. 2 Sketches used for deriving and interpreting the stress equations

$$\frac{N_\phi}{r_1} + \frac{N_\theta}{r_2} = p \tag{6}$$

Eq. (6) is derived in the references previously cited (e.g. Eq. (2.4) of Haas, 1962; Eq. (10.1a) in Ugural, 1981; Eq. (2.6c) of Flügge, 1973). The derivation of Eq. (6) is omitted because it is lengthy, because we could not improve on the derivation of others, and because it is common (e.g. see Fung, 1993). Since Eq. (6) has two unknown stresses, another equation is needed. This equation was found by applying x-direction equilibrium to the portion of the model AAA shown in Fig. 2(e):

$$p\pi(y^2 - r_v^2) + T(x) - N_\phi 2\pi y \sin\phi = 0. \tag{7}$$

Note that T is a resultant force which can characterize an arbitrary distribution of longitudinal tethering forces. Letting $\sin\phi = y/r_2$ and rearranging Eq. (7) gives

$$N_\phi = \frac{r_2}{2\pi y^2}[\pi p(y^2 - r_v^2) + T(x)]. \tag{8}$$

Normalization of the Stress Equations. To normalize stress, we used the hoop stress in a round, open-ended, straight tube of radius r_v. When such a tube is subjected to a uniform internal pressure p, the resultant product of hoop stress and wall thickness is pr_v. Hence, normalized stresses are defined by

$$N_\phi^* \equiv \frac{N_\phi}{pr_v}, \quad \text{and} \quad N_\theta^* \equiv \frac{N_\theta}{pr_v}, \tag{9}$$

where the (*) notation indicates that the term is normalized. Similarly, to normalize lengths, we used r_v:

$$y^* \equiv y/r_v, \quad r_1^* \equiv r_1/r_v, \quad \text{etc.} \tag{10}$$

Note that $r_v = 1$ cm; hence, normalized lengths equal actual lengths (i.e. if $y^* = 1$, then $y = 1$ cm). Substituting Eqs. (9) and (10) into Eqs. (6) and (8) gives

$$\frac{N_\phi^*}{r_1^*} + \frac{N_\theta^*}{r_2^*} = 1, \quad \text{and} \tag{11}$$

$$N_\phi^* = \frac{r_2^*}{2y^{*2}}[(y^{*2} - 1) + T^*], \tag{12}$$

where $T^* = T/(\pi r_v^2 p)$. Eqs. (11) and (12) are the desired result.

Results

To simplify the notation, results are presented without the (*) notation. This presentation begins with a very simple case, the open-sphere model with T set to zero.

The Open-Sphere Model. The open-sphere model is shown in Fig. 3(a). The x-axis gives axial location as measured from the bulge center. As previously stated, the axis scale, while dimensionless, can be interpreted in units of centimeters. Similarly, the curve $y(x)$ can be interpreted in centimeters, with numerical values indicated on the vertical axis. Hence, the open-sphere shape can be interpreted as a spherical shaped aneurysm with a bulge diameter of 5 cm.

Also shown in Fig 3(a) are the calculated hoop and meridional stress distributions. Normalized stress values can be interpreted as

$$\text{Normalized Stress} = \frac{\text{Stress in the AAA Model}}{\text{Hoop Stress in a Normal Aorta}}, \tag{13}$$

where the denominator of Eq. (13) becomes (because of the model assumptions) the hoop stress in a round, open-ended, straight tube. Hence, the hoop stress at the bulge center equals about 150 percent of the hoop stress in the end tube. Notice

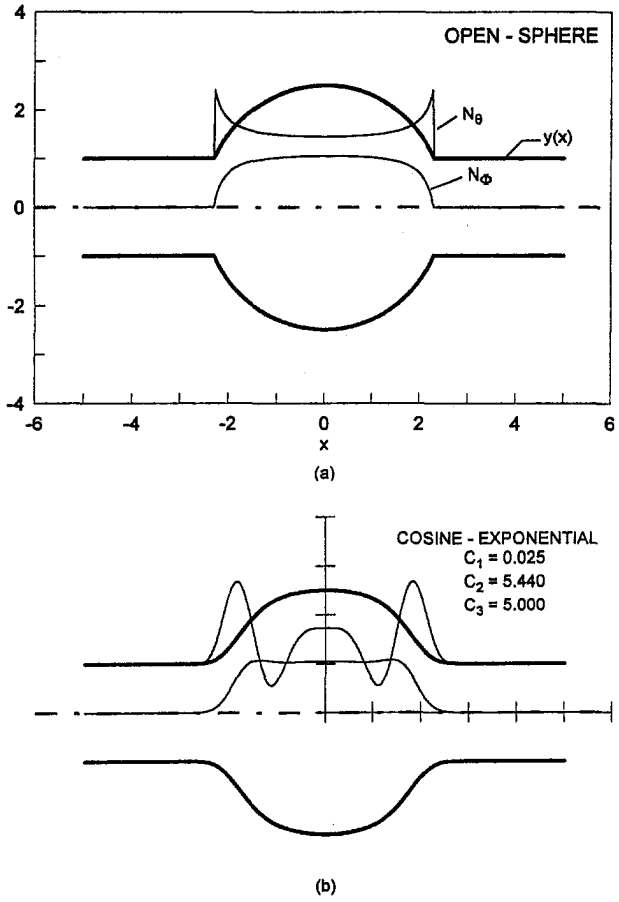

Fig. 3 Stress fields for two AAA models, each with $T = 0.0$

that for $x \geq \approx 2.3$, both stresses return to the values for the tube (namely, $N_\phi = 0.0$ and $N_\theta = 1.0$).

The hoop stress displays a discontinuity at the junction of the sphere and the end tube. This discontinuity and other features of the stress fields can be explained by using the equilibrium equations. From x-direction equilibrium (see Fig. 2(e)), the meridional force must balance the excess pressure force. The excess pressure force occurs because the left face section area (πy^2) exceeds the right face section area (πr_v^2). As x ranges from 0 to L, this difference in section areas decreases from a maximum value to zero. In the same fashion, N_ϕ decreases from a maximum value to zero. The hoop stress distribution $N_\theta(x)$ can be explained using normal direction equilibrium (i.e. eq. 11). For the sphere portion of the shape, $r_1 = r_2 = 2.5$, and Eq. (11) reduces to

$$N_\phi + N_\theta = 2.5. \tag{14}$$

Because $N_\phi(x)$ decreases with increasing x, $N_\theta(x)$ must increase to satisfy Eq. (14).

The discontinuity in N_θ at $x \approx 2.3$ occurs because r_2 has a step change from 2.5 to 1.0 at this location. As shown by Eq. (5), the step change in r_2 occurs because the first derivative of $y(x)$ is discontinuous. Because such a change in slope is unlikely to occur in vivo, an AAA model with a discontinuous wall slope is inappropriate for idealizing an AAA. Note that the AAA shapes shown in Stringfellow et al.'s (1987) study had discontinuous wall slopes. Not surprisingly, the corresponding stress distributions of Stringfellow et al. show N_θ discontinuity, just like Fig. 3(a).

In conclusion, the meridional curve used to generate the AAA model should have a continuous first derivative. In addition, a continuous second derivative is also needed. This is because a discontinuity in the second derivative will cause a discontinuity in r_2, a result which is evident from Eq. (2). All subsequent shapes have continuous first and second derivatives, ensuring that singularities do not influence the predicted stresses.

The Cosine-Exponential Shape. This shape approximates the open sphere shape with an appropriate meridional curve. The resulting stress distributions are shown in Fig. 3(b). To simplify this and subsequent figures, the graph labeling scheme was simplified. Notice that N_ϕ, N_θ and $y(x)$ are unlabeled; this is because $y(x)$ is obvious, and because N_θ and N_ϕ are easy to discern (maximum N_θ is always larger than N_ϕ; see Fig. 3(a)). Also, regarding the x and y-axes, each tick mark equals one unit, and the axis are shifted to the interior of the AAA model. In comparing the open sphere shape to the cosine-exponential shape, notice that both the shapes and the N_ϕ distributions are quite similar. The reason for the N_ϕ similarity is that the x-direction forces and ensuing equilibrium were virtually the same. In contrast, the N_θ distributions differed considerably, a result which occurred because surface curvatures differ between the two shapes. To visualize this point, notice that normal-direction equilibrium shows that $N_\theta/r_2 + N_\phi/r_1$ balances pressure, a concept which can be inferred from Fig. 2(d). Because the principal curvatures cause N_ϕ and N_θ to have components in the direction of pressure, the magnitudes of $r_1(x)$ and $r_2(x)$ essentially determine $N_\theta(x)$.

Notice in Fig. 3(b) that $N_{\theta,\max}$ occurred near the inflection point of $y(x)$. At inflection, $r_1 \rightarrow \infty$ because the meridional curve was changing from downward curvature to upward curvature. Hence at inflection, $N_\phi(x)/r_1 = 0$, and pressure was balanced by the hoop stress only, causing $N_{\theta,\max}$ to occur near the inflection point of $y(x)$. For most of the shapes studied, the inflection point had a dominant influence on the location and magnitude of the maximum stress.

The Influence of Vascular Tethering. All results so far have been presented with tethering set to zero. However, it is well known that arteries are loaded by a longitudinal tethering force. To estimate this force, some have multiplied systolic pressure by cross sectional area (e.g. Dobrin 1989). However, since the vessel is not closed, we believe that this estimate is much too high. Thus, T was estimated as $T = k\delta$, where k is a spring constant which represents the longitudinal stiffness of the abdominal aorta, and δ is a change in length from the unstressed position. To estimate δ, we assumed that the abdominal aorta when excised from the body would shrink less than 30 percent (more likely about 10 percent). To estimate k, canine data from Patel and Fry (1966) were used. Since these data are presented on a per volume basis, they should be reasonable for estimating values for human vascular tissue. From Patel and Fry's (1966) results, the value of $k = 16$ N/m was calculated. Now, when the abdominal aorta shrinks by 30 percent in length, $\delta \approx 2.5$ cm, giving a value of the tethering force of $k\delta = 0.40$ N. To normalize this value, a systolic pressure of 18 kPa acting over a 1.7-cm-diameter exerts a force of about 4 N, giving a normalized value of tethering of about 0.1.

The effects of T on the stress distribution for two shapes are shown in Fig. 4. As compared to zero tethering, a tethering of $T = 0.1$ caused only slight changes in the stresses. Even when the tethering force was set to a very high value ($T = 1.0$) the stresses were influenced only moderately. Because $T = 0.1$ was likely an overestimate, it seemed apparent that tethering forces only slightly influenced the wall stresses. All remaining results will be presented with $T = 0.1$.

The Influence of Model Shape on Stress Distribution. To illuminate how AAA shape and stress are related, stresses were calculated for a series of different shapes, each with bulge diameter held constant at $D_b = 5.0$ (Fig. 5). The results in Fig. 5 illustrate that the distribution of hoop stress is strongly influenced by AAA shape. Moreover, the maximum stress, which

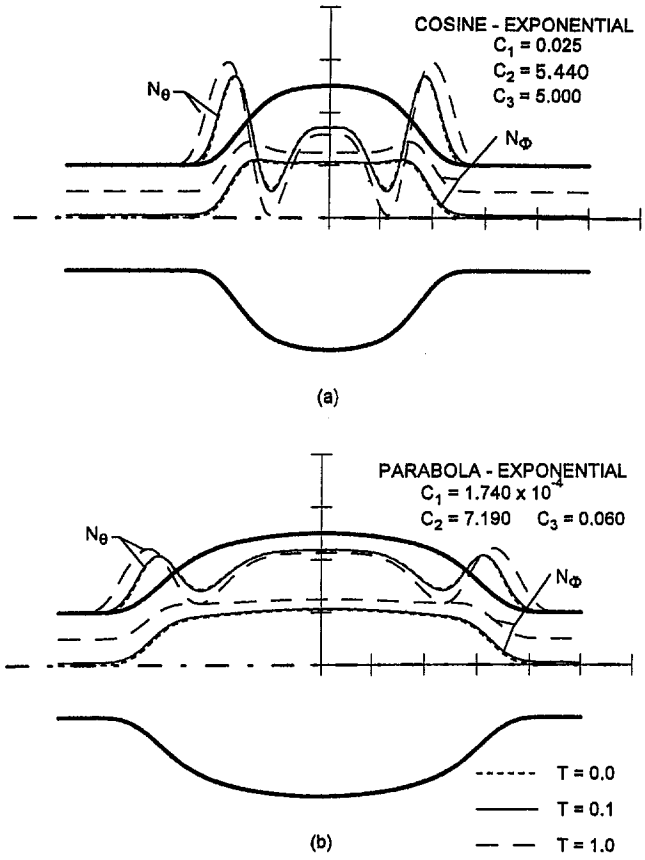

Fig. 4 The effect of T on the stress distributions for two AAA models

ranges from 2.0 to 3.2, is also strongly dependent on AAA shape. Regarding this later point, notice that those shapes with the smallest curvatures (5(a) and 5(c)) have the highest $N_{\theta,\max}$.

Another way to assess the influence of shape is to hold $N_{\theta,\max}$ constant and vary D_b (Fig. 6). While all shapes in Fig. 6 have the same maximum stress ($N_{\theta,\max} = 3.0$) the bulge diameters vary from $D_b = 4.18$ to $D_b = 7.00$. In conclusion, it is very evident that maximum hoop stress is significantly influenced by AAA shape, a result suggesting that present clinical practice—i.e., predicting rupture using D_b only--can be substantially improved.

Implication of the Present Results to Current Clinical Practice. When the law of Laplace was applied to the results in Fig. 6, $N_{\theta,\max}$ values ranged from 1.05 to 1.75 (Table 1). These values lie well below the true value of $N_{\theta,\max} = 3.00$, with the worst prediction off by nearly a factor of three! Moreover, the law of Laplace predicted that the hoop and meridional stresses were equal and independent of axial location. It is obvious that the law of Laplace is simply not close, neither qualitatively nor quantitatively.

Because $N_{\theta,\max}$ was not well correlated with D_b, we used Eq. (11) to estimate that

$$\frac{N_{\theta,\max}}{r_{2,I}} = 1, \tag{15}$$

where the subscript "I" denotes the inflection point, and N_ϕ / r_1 does not appear because $r_1 \to \infty$ at inflection. Eq. (15) predicts $N_{\theta,\max}$ with about 90 percent accuracy (Table 1).

If more accuracy is desired, Eq. (15) can be improved. In particular, $N_{\theta,\max}$ does not occur exactly at the inflection point, but is shifted toward the end of the AAA. Thus, we assumed that maximum stress occurs at a point "P," which is shifted by 0.05 from inflection. Using Eq. (12) with a normalized tethering of 0.1 gave an estimate of $N_{\phi,P}$:

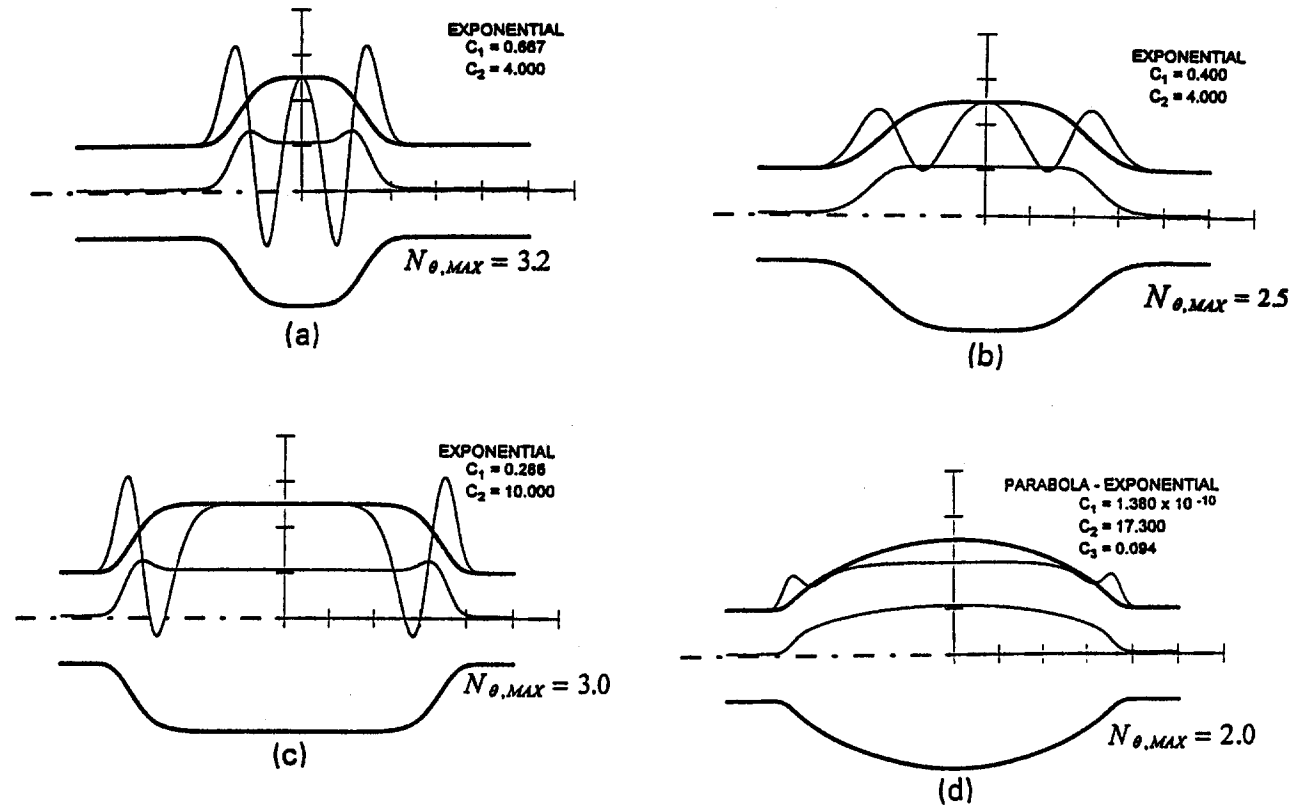

Fig. 5 Stress distributions for various AAA models, each with $T = 0.1$ and $D_b = 5.0$

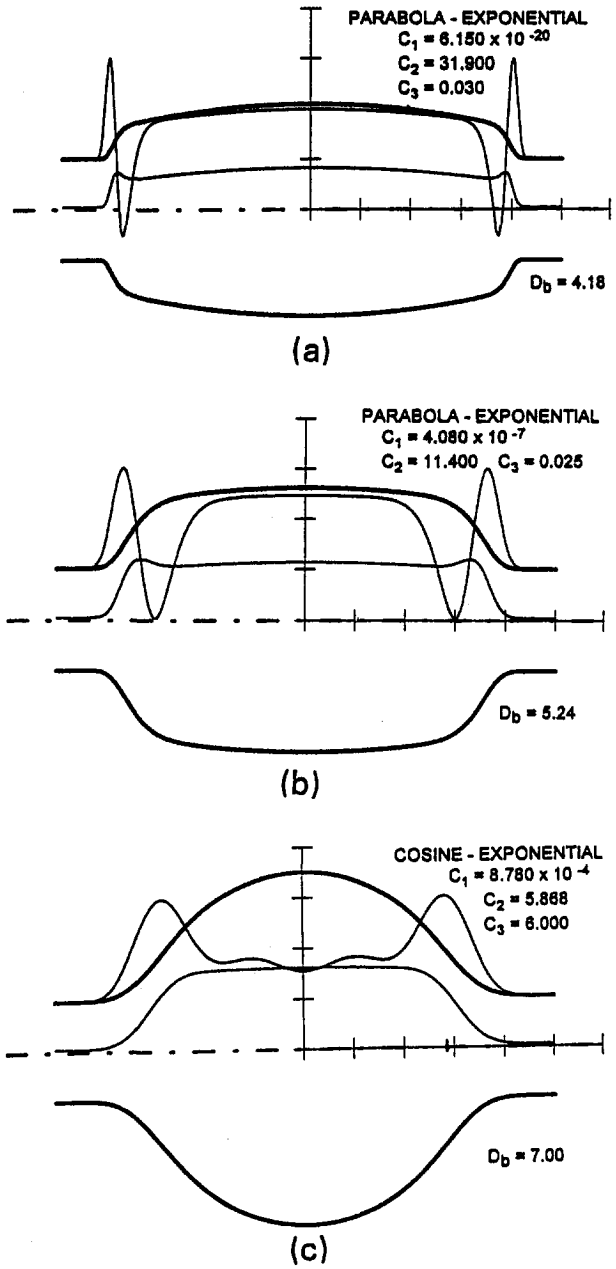

Fig. 6 Stress distributions for three AAA models, each with $T = 0.1$ and $N_{\theta,\max} = 3.00$

$$N_{\phi,P} = \frac{r_{2,P}}{2y_P^2}(y_P^2 - 0.9), \qquad (16)$$

Then by using Eq. (11), $N_{\theta,\max}$ was estimated as

$$N_{\theta,\max} = r_{2,P}\left(1.0 - \frac{N_{\phi,P}}{r_{1,P}}\right). \qquad (17)$$

Table 1 shows that Eq. (17) predicted the maximum stress with better than 99 percent accuracy. However, the aim here is not to prove that Eq. (15) or (17) is the best way to predict rupture. Rather, the aim is to suggest that use of parameters other than D_b may lead to improved prediction of rupture. There are two very important details to notice about Eqs. (15) to (17). First, the parameters which appear in these equations can be found from clinical imaging data. Second, D_b does not appear in the equations, a fact which implies that wall curvatures--not bulge diameter--have the primary influence on the maximum stress. This idea suggests that rupture probability should be based on wall curvatures, not bulge diameter. Of course this idea was rather unexpected--for many years, physicians have used bulge diameter to predict AAA rupture. However, there is no contradiction because D_b and wall curvatures are related: D_b appears in $y(x)$, and $y(x)$ is used to calculate curvatures. Nevertheless, the message in the math is clear--the maximum stress is directly influenced by wall curvatures and D_b has only a secondary influence.

In closing, it is appropriate to emphasize that our results apply to a model AAA, a model developed using many simplifying assumptions, introducing several possible ways in which our results could be modified. For example, significant wall thickness variations would greatly alter stress distributions. Similarly, residual stresses could alter stress distributions. Geometric effects associated with more realistic shapes could also influence predicted stresses. If the AAA wall is carrying a significant portion of the applied load with bending stresses, this could introduce significant stress variations through the AAA wall thickness. Finally, the location of rupture could be significantly influenced by local variations in the strength of the AAA tissue.

Conclusions

Our aim was to determine how stresses acting in AAA walls correlated with the shape of the AAA. To analyze this problem, we applied membrane theory to a model AAA and reached the following conclusions:

- The meridional stresses were typically two to three times smaller than the maximum hoop stress.
- Regarding the stress distributions, the shape of the AAA had a small effect on the meridional stresses and a rather dramatic effect on the hoop stresses. Thus, AAA shape had a very significant influence on the maximum stress.
- Tethering forces had only a small influence on stress magnitudes and distributions.
- Maximum stress typically occurred near the inflection point of a curve drawn coincident with the AAA wall.

The stress analysis showed that the law of Laplace provided neither qualitative nor quantitative understanding of the stresses in an AAA. Moreover, the maximum stress did not even directly

Table 1 Prediction of $N_{\theta,\max}$ for the data shown in Fig. 6

		Data from Fig. 6						Prediction of $N_{\theta,\max}$		
ID	Location	x	y	r_1	r_2	N_ϕ	N_θ	Law of Laplace Eq. (1)	Eq. (15)	Eq. (17)
6*a*	inflection	3.976	1.256	∞	2.695	0.581	2.681	1.046	2.695	3.001
	at x_p	4.026	1.165	−1.456	2.358	0.397	3.001			
6*b*	inflection	3.573	1.567	∞	2.926	0.927	2.920	1.310	2.926	2.997
	at x_p	3.623	1.489	−9.490	2.759	0.819	2.997			
6*c*	inflection	2.820	1.931	∞	3.002	1.139	3.001	1.751	3.002	2.992
	at x_p	2.870	1.871	−36.06	2.905	1.079	2.992			

depend on AAA bulge diameter. Rather, maximum stress correlated with AAA wall curvatures (i.e., shape). This result suggested that using AAA bulge diameter to predict AAA rupture is not well founded. A better concept is to relate the probability of AAA rupture to wall curvatures.

To provide additional insights, future analyses will add additional physiological realism to the AAA model, a modeling effort which may consider non-symmetric shapes, the influences of both wall thickness and wall thickness variations, and the coupling of hemodynamics and wall motions during the cardiac cycle. The ultimate goal is to provide improved clinical definitions of AAAs which have an especially high risk of rupture. Such knowledge, when coupled with accurate imaging technology, could greatly improve the prognostication of AAA rupture.

References

Bernstein, E. F., Dilley, R. B., Goldberger, L. E., Gosink, B. B., and Leopold, G. R., 1976, "Growth Rates of Small Abdominal Aortic Aneurysms," *Surgery,* Vol. 80(6), pp. 765–773.

Brown, P. M., Pattenden, R., and Gutelius, J. R., 1992, "The Selective Management of Small Abdominal Aortic Aneurysms: The Kingston Study," *J. Vasc. Surg.,* Vol. 15, pp. 21–27.

Cronenwett, J. L., Murphy, T. F., Zelenock, G. B., Whitehouse, W. M., Lindenauer, S. M., Graham, L. M., Quint, L. E., Silver, T. M., and Stanley, J. C., "Actuarial Analysis of Variables Associated with Rupture of Small Abdominal Aortic Aneurysms," *Surgery,* Vol. 98(3), pp. 472–483.

Dobrin, P. B., 1989, "Pathophysiology and Pathogenesis of Aortic Aneurysms," *Surg. Clin. of N. Amer.,* Vol. 69, pp. 687–703.

Drexler, D. J., and Hoffman, A. H., 1985, "Steady Flow Through Several Aneurysm Models," *Proceedings of the Eleventh Annual Northeast Bioengineering Conference,* W. Kuklinski and W. Ohley, eds., pp. 147–150.

Dubost, C., Oeconomos, N., Allary, M., 1952, "Resection of an Aneurysm of the Abdominal Aorta," *Arch. Surg.,* Vol. 64, p. 405.

Estes, J. E., 1950, "Abdominal Aortic Aneurysm: A Study of One Hundred and Two Cases," *Circulation,* Vol. II, pp. 258–264.

Faggioli, G. L., Stella, A., Gargiulo, M., Tarantini, S., D'Addato, M., Ricotta, J. J., 1994, "Morphology of Small Aneurysms: Definition and Impact on Risk of Rupture," *Am. J. Surg.,* Vol. 168, pp. 131–135.

Flügge, W., 1973, *Stresses in Shells,* 2nd Ed., Springer-Verlag, New York, pp. 1–100.

Fung, Y. C., 1993, *Biomechanics: Mechanical Properties of Living Tissues, 2nd Ed.,* Springer-Verlag, New York.

Gaylis, H., 1983, "Evaluating the Size of an Aneurysm," *Surgery,* pp. 324–325.

Haas, 1962, *Thin Concrete Shells: Vol. 1,* Wiley, New York, pp. 1–29.

Hollier, L. H., Taylor, L. M., Ochsner, J., 1992, "Recommended Indications for Operative Treatment of Abdominal Aortic Aneurysms," *J. Vasc. Surg.,* Vol. 15(6), pp. 1046–1056.

Horwitz, O., McCombs, P., and Roberts, B., 1985, *Diseases of Blood Vessels.* Lea & Febiger, Philadelphia.

Hunter, G. C., Leong, S. C., Yu, G. S. M., McIntyre, K. E., and Bernhard, V. M., 1989, "Aortic Blebs: Possible Site of Aneurysm Rupture," *J. Vasc. Surg.,* Vol. 10, pp. 93–99.

Johansen, K. H., 1982, "Aneurysms," *Scientific American,* Vol. 247, pp. 110–125.

Katz, D. A., Littenberg, B., Cronenwett, J. L., 1992, "Management of Small Abdominal Aortic Aneurysms: Early Surgery vs. Watchful Waiting," *JAMA,* Vol. 268(19), pp. 2678–2686.

Kerstein, M. D., Moulder, P. V., and Webb, W. R., 1983, *Aneurysms.* Williams & Wilkins, Baltimore.

Langewouters, G. J., Wesseling, K. H., and Goedhard, W. J. A., 1984, "The Static Elastic Properties of 45 Human Thoracic and 20 Abdominal Aortas In Vitro and the Parameters of a New Model," *J. Biomechanics,* Vol. 17, pp. 425–435.

Michaels, J. A., 1992, "The Management of Small Abdominal Aortic Aneurysms: a Computer Simulation Using Monte Carlo Methods," *Eur. J. Vasc. Surg.,* Vol. 6, pp. 551–557.

Milnor, W. R., 1989, Hemodynamics, Williams and Wilkins, Baltimore, pp. 58–101.

Mower, W. R., Baraff, L. J., and Sneyd, J., 1993, "Stress Distributions in Vascular Aneurysms: Factors Affecting Risk of Aneurysm Rupture," *J. Surg. Res.,* Vol. 55, pp. 155–161.

Patel, D. J., Fry, D. L., 1966, "Longitudinal Tethering of Arteries in Dogs," *Circ. Res.,* Vol. 19, 1011–1021.

Stringfellow, M. M., Lawrence, P. F., and Stringfellow, R. G., 1987, "The Influence of Aorta-Aneurysm Geometry Upon Stress in the Aneurysm Wall," *J. Surgical Res.,* Vol. 42, 425–433.

Ugural, A. C., 1981, *Stresses in Plates and Shells,* McGraw Hill, New York, pp. 198–205.

US Government, 1991, *Vital Statistics of the United States,* US Government Printing Office: Washington, D.C.

Veldenz, H. C., Schwarcz, T. H., Endean, E. D., Pilcher, D. B., Dobrin, P. B., and Hyde, G. L., 1994, "Morphology Predicts Rapid Growth of Small Abdominal Aortic Aneurysms," *Ann. Vasc. Surg.,* Vol. 8, pp. 10–13.

APPENDIX A:

Mathematical Details of the Meridional Curves

Each model AAA was developed by rotating a meridian curve $y(x)$ about the x-axis, Fig. $1(b)$. These curves were developed using analytical equations. The reason for analytical equations, as opposed to pointwise data, was that the second derivatives could be found with precision. The first shape selected was the "open-sphere" shape, pictured in Fig. $3(a)$. The meridional curve equation for this shape is

$$y(x) = \sqrt{r_b^2 - x^2}: \quad \text{if} \quad |x| < \sqrt{r_b^2 - r_v^2},$$
$$y(x) = r_v: \quad \text{otherwise.} \tag{A.1}$$

As shown in Fig. $3(a)$ and discussed in the text, this shape had obvious problems because the slope of the meridional curve was not continuous.

To satisfy the continuity requirements on the meridional curve and its derivatives, we selected "the exponential shape," a modification of the Gaussian distribution:

$$y(x) = (r_b - r_v)e^{-|C_1 x/r_v|^{C_2}} + r_v, \tag{A.2}$$

where C_1 and C_2 are adjustable parameters which can be varied to produce a variety of different shapes, Figs. $5(a)$–$5(c)$.

Because many realistic shapes cannot be reproduced with the exponential shape, we next searched for other suitable analytical functions: this effort was not successful. Then, it was noticed that the exponential function, because it behaves like an "on/off switch," could be used to develop other shapes. For example, the function $f(x)$,

$$f(x) = e^{-C_1|x/r_v|^{C_2}} \tag{A.3}$$

with a suitable choice of the parameters C_1 and C_2 has a value of 1.0 over most of the AAA bulge region and a value of nearly zero otherwise. Now, the function $g(x)$,

$$g(x) = (r_b - r_v) - C_3 x^2/r_v \tag{A.4}$$

with a suitable choice of the parameter C_3, gives a good approximation of an AAA bulge, but fails to merge into the proximal and distal arteries. However, the product of $f(x)$ and $g(x)$ gives an excellent AAA shape:

$$y(x) = f(x)g(x) + r_v \tag{A.5}$$
$$= e^{-C_1|x/r_v|^{C_2}}[(r_b - r_v) - C_3(x^2/r_v)] + r_v.$$

Eq. (A.5) has the requisite continuous first and second derivatives, and gives an excellent shape; in particular, the "Parabola-Exponential" shape. Using the idea of the parabola-exponential shape, the final shape used for analysis is the "cosine-exponential shape," given by

$$y(x) = e^{-C_1|x/r_v|^{C_2}}\left[\frac{(r_b - r_v)}{2}\left(\cos\left(\frac{\pi x}{C_3 r_v}\right) + 1.0\right)\right] + r_v. \tag{A.6}$$